GEOPHYSICS, VOL. 71, NO. 4 (JULY-AUGUST 2006); P. G179–G189, 9 FIGS.
10.1190/1.2217367

Electrical-prospecting method for hydrocarbon search using the induced-polarization effect

Sofia Davydycheva[1], Nikolai Rykhlinski[2], and Peter Legeido[3]

ABSTRACT

We propose a method of surface and marine electrical prospecting using controlled-source excitation. The method is designed to detect hydrocarbon deposits at depths of a few kilometers and to map their boundaries. The technique is based on imaging the induced-polarization (IP) parameters of the geologic formation. We use the fact that, because of the imaginary part of the electric conductivity, polarized media support wave propagation processes whose nature is similar to displacement currents induced by the dielectric permittivity. However, unlike displacement currents, these processes reveal themselves at much lower frequencies and, therefore, at greater depths. It is established that the ratio of the second and the first differences of the electric potential does not decay after the current turn-off in polarized media, whereas it decays quickly if the IP effect is absent. Thus, the IP response can be observed directly and separated from the electromagnetic (EM) response. We use a vertical focusing of the electric current to decrease the effect of laterally adjacent formations to apply a 1D layered model in a 3D environment. This method obtained promising results in several regions of Russia.

INTRODUCTION

In spite of the progress in seismic prospecting methods for investigating geologic structures associated with oil or gas reservoirs, the percentage of productive wells has remained low from year to year. The mean value of this quantity when using 2D seismic is about 30%. Obtaining additional independent geologic information that could help to increase the success rate of oil- and gas-well drilling is a great economical problem.

Some electrical-resistivity prospecting methods use controlled-source excitation. Both frequency- and transient-electromagnetic (EM) soundings (Vanyan, 1965) have been used to determine formation resistivity. However, general experience has shown that EM methods are usually insufficient for direct exploration of oil deposits because in most cases oil-saturated rocks are also saturated with mineralized groundwater, so the difference between the electrical resistivities of oil- and water-bearing rocks is not large enough to be detected. These methods have rather low spatial resolution and provide spatially averaged information about the formation.

However, it was established that the electrical conductivity of sedimentary rocks depends on the exciting frequency of the EM field, as a result of the induced-polarization (IP) effect. Since the discovery of the IP effect (Schlumberger, 1920; Allaud and Martin, 1977), numerous attempts have been made to apply it to electrical surveys (Seigel, 1974; Dey and Morrison, 1973) and resistivity logging (Freedman and Vogiatzis, 1986). However, the nature of this electrochemical phenomenon is rather complicated and not completely understood.

Fuller and Ward (1970) describe frequency-dependent electrical properties in terms of complex conductivity or complex permittivity. They suggest three mechanisms for a large polarization effect in rocks: electrode polarization, membrane polarization, and interfacial polarization.

Three principal types of water-mineral physicochemical reactions can cause the IP effect (Marshall and Madden, 1959; Olhoeft, 1985). The processes resulting from corrosion of metallic minerals such as pyrite or magnetite are well studied by electrochemists and metallurgists, and are used widely for revealing ore deposits (Mikhailov et al., 1973). Exchange reactions in clay and shaley sands are not so well studied (Klein and Sill, 1982; Ulrich and Slater, 2004). Nevertheless, they are used for hydrogeologic purposes (Komarov, 1980; Slater and Glaser, 2003). The least studied and the most complicated case is related to the reactions involving organic materials. Olhoeft (1985) states that organic contamination of rocks shifts the EM-field phase response to lower frequencies. Kemna et al. (2004) report an

Manuscript received by the Editor June 15, 2003; revised manuscript received November 2, 2005; published online August 8, 2006.
[1]Formerly Central Geophysical Expedition, Moscow, Russia; presently Schlumberger, Sugarland Product Center, 110 Schlumberger Drive, MD5 Sugar Land, Texas 77478. E-mail: sdavydycheva@slb.com.
[2]Institute of Innovative Methods of Geophysics, Zhadova Generala pl., 7, 123098 Moscow, Russia. E-mail: rykhlinski@mail.ru.
[3]State Enterprice "Irkutskgeofizika", Clara Tsetkin ul., 9, Irkutsk 664039, Russia.

increased imaginary conductivity in the presence of hydrocarbons. Pirson (1982) suggests the following explanation of the electrochemical phenomena occurring when hydrocarbons are present. He assumes that during the migration of hydrocarbons, the mineralized water changes its chemical properties and acquires alkaline properties. Thus, a reduced zone appears in the area of the oil reservoir that increases the intensity of electrochemical reactions.

Many authors have proposed different empirical and phenomenological models describing the IP effect: Cole-Cole model, Dias model, Debye model, Warburg model, Davidson-Cole model, Wait model, etc. (see detailed reviews by Dias, 2000, and Komarov, 1980). All models imply that complex electric conductivity depends on frequency, particularly at low frequencies from 0.1 to 1000 Hz.

Because of the IP effect, an out-of-phase or quadrature conductivity appears in saturated sedimentary rocks (Vinegar and Waxman, 1984). This means that an effective dielectric permittivity arises that can exceed many times the vacuum value. Freedman and Vogiatzis (1986) claim that the effective permittivity can be more than six orders of magnitude greater than the dielectric constant of vacuum.

One electrical-survey method that makes use of the IP effect is the phase method of induced polarization (Kulikov and Shemyakin, 1978). In this method, phase shift — denoted by φ_{IP}, between the voltages of the transmitter and the receiver — is used for interpretation. Subtracting signals at two exciting frequencies is used to suppress the EM induction effect. With such an approach, a hydrocarbon deposit can be visualized as a zone of anomalous φ_{IP}. This method is successful only in the case when some metallic minerals, such as pyrite, accompany the oil deposit. However, if they are absent, the abnormality of φ_{IP} is generally not large enough, and it provides only crudely averaged information about the formation. Sometimes the signature of the deposit is indirectly mapped into φ_{IP} because of halo diffusion of hydrocarbons in the column of overlying rocks, including the near-surface rocks. Rocks exhibiting hydrocarbon diffusion may be displaced with respect to the deposit because of migrating lighter hydrocarbons along faults and other heterogeneities.

Let us quote the opinion of James R. Wait (1982, p.194):

> A final and still unresolved question in transient electromagnetic sounding of the earth's crustal layers is the significance of induced polarization. Even with an ungrounded inductive system, the frequency dispersion of the complex resistivity of the constituent media will influence the time-domain response. The untangling of the IP and EM responses is a task that has not yet been completed. Ultimately, the dual role of these phenomena in any electromagnetic exploration system should be exploited as a source of rich information about the environment.

In this paper, we propose a method for the task of direct search and delineation of hydrocarbon deposits that provides the possibility of untangling the EM and IP responses of the formations.

THEORETICAL BACKGROUND

The suggested method (Rykhlinski et al., 2003, 2004a, 2004b, 2004c) is based on using current pulse excitation of the electromagnetic field and a differential-normalized method (DNM) for receiving and processing the sounding signals.

Consider the frequency-domain equation for the electric field $\mathbf{E}$:

$$\nabla \times \nabla \times \mathbf{E}(i\omega) - i\omega\mu\sigma\mathbf{E}(i\omega) + \omega^2\mu\epsilon\mathbf{E}(i\omega) = i\omega\mu\mathbf{j}_0(i\omega). \quad (1)$$

This can be obtained from the time-domain Maxwell's equations

$$\nabla \times \mathbf{H} = \mathbf{j}_0(t) + \mathbf{j}(t) + \varepsilon\frac{\partial \mathbf{E}}{\partial t},$$

$$\nabla \times \mathbf{E} = -\mu\frac{\partial \mathbf{H}}{\partial t}, \quad (2)$$

by eliminating the magnetic field $\mathbf{H}$, provided that the exciting current density $\mathbf{j}_0(t) \sim e^{i\omega t}$. Here ε is the dielectric permittivity of the medium, μ is its magnetic permeability, and $\mathbf{j}(t)$ is the conductivity current density, which obey the following generalized Ohm's law:

$$\mathbf{j}(t) = \int_{-\infty}^{t} \sigma(\tau)\mathbf{E}(t-\tau)d\tau \quad (3)$$

(Kulikov and Shemyakin, 1978). Equation 3 shows that, in the form of a convolution integral, the current density $\mathbf{j}$ at moment t is connected with the conductivity and the electric field $\mathbf{E}$ at all previous moments of time. The convolution occurs because of the accumulation of electric charges and creation of electric double layers on liquid-mineral interfaces within polarized media. The generalized Ohm's law in the frequency domain has the form

$$\mathbf{j}(i\omega) = \sigma(i\omega)\mathbf{E}(i\omega), \quad (4)$$

because the Fourier transform of the convolution of two variables is the product of their Fourier transforms.

We use an empirical model of the electric conductivity proposed by Cole and Cole (1941) and applied by Pelton et al. (1978) to the IP effect:

$$\sigma(i\omega) = \sigma_0\left(1 - \frac{\eta}{1 + (i\omega\tau)^c}\right), \quad (5)$$

where η is the IP coefficient (also known as the intrinsic chargeability of sedimentary rocks), τ is the time decay constant of the IP potential, and c is the relaxation constant. Usually, $0 \le c \le 1$, whereas the coefficient of sedimentary rocks η does not exceed 0.1. The time-decay constant τ varies in the range of seconds and dozens of seconds in the presence of electronic-conductive rocks (ore deposits); however, for ionic-conductive rocks, τ usually does not exceed a few tenths of a second (Komarov, 1980). Note that the original Cole-Cole formula for resistivity differs from equation 5; however, they are equivalent (Kormil'tsev and Mezentsev, 1989, 22).

If $\eta \neq 0$, $\tau \neq 0$, and $c > 0$, the conductivity in equations 5 and 1 becomes complex. This means that equation 1 contains a term proportional to ω^2 because of the imaginary part of the conductivity, even under the assumption that $\epsilon = 0$ (this is usually assumed at low frequencies when $\sigma \gg \omega\epsilon$). We can find the new ω^2-dependent term by expanding the conductivity (equation 5) in a Taylor series in powers of $(\omega - \omega_0)$, where ω_0 can be chosen depending on the excitation current.

Thus, equation 1 no longer can be considered a diffusion equation, even at very low frequencies. In other words, because of the IP effect, the alternating low-frequency electromagnetic field penetrates the formation not only because of the diffusion currents caused by

the real part of the conductivity σ, but also, because of displacement currents caused by the induced polarization of the rocks.

Thus, because of the IP effect, polarized beds behave similarly to giant capacitors. They accumulate electric potential energy when the energizing current is turned on, and then, similarly to capacitors, slowly release it during the off-time. This is why the electric field decay time after current turn-off is much slower in polarizable than in unpolarizable media (Dey and Morrison, 1973). When measuring certain differential data, as described below, this slow decay time can be directly observed and associated with the depths and properties of the responding beds.

Therefore, the ability of an electrical survey to image formation properties using a low-frequency pulse current may be greater than traditionally held. However, this ability can be realized only if the number of measured data is at least equal to the number of parameters to be estimated by inversion, and if the data are independent of each other.

For IP studies, most authors use conventional apparent resistivity

$$\rho_{\text{app}} = K\frac{\Delta U}{I}, \tag{6}$$

where ΔU is the potential difference or the voltage in the receiver, I is the transmitter current, and K is the calibration factor of the tool. For example, Seigel (1959, 1974) investigated ρ_{app} for ungrounded magnetic dipoles, whereas Dey and Morrison (1973) used grounded pole-dipole and dipole-dipole systems.

Nevertheless, neither the apparent conductivity nor the phase shift is able to provide complete information about the electric properties of the polarizable formations that should be described by at least four independent parameters: σ_0, η, τ, and c.

EXPERIMENTAL SETUP

Two grounded dipole current transmitters oriented along the horizontal x-axis, as depicted in Figure 1a, excite an electromagnetic field inside the formation. The moments of the dipoles are opposite to each other. The distance between them can vary from 1 to 10 km. The dipole lengths vary from 200 m to 2 km. A receiver consisting of three equidistant grounded electrodes is placed at the midpoint between the transmitters so that the first and second spatial differences of the electric potential can be measured. Obviously, if U is the potential of the electric field, then the voltmeter depicted in Figure 1a measures the voltage $(U_1 - 2U_2 + U_3)/2$, which is the second potential difference between electrodes 1, 2, and 3 (numbered in a consequent order) divided by two. Thus, the depicted receiver is, in effect, a quadrupole having two negative (internal) poles colocated. Figure 1b and c show the dc distribution in a homogeneous half-space for the transmitters and the receiver, respectively.[4]

It is easy to see that the axial current, which is strong in the vicinity of each transmitter, can be negligibly small in the area of the receiver so that the vertical current prevails in the formation below the receiving electrodes. Moreover, the second potential difference $\Delta_x^2 U$ measured by the receiver is proportional to the total vertical current below it. Zhdanov and Keller (1994, 369, equation 7.104) show that in the case of transient processes in a homogeneous half-space, the y-component of the current density j_y is equal to 0 after the current turn-off, not only on the dipole axis x (i.e., at $y = 0$), but in every point on the earth's surface. Unlike j_x, the y-component j_y contains only a geometrical factor and Heaviside step function as the only time-dependent factor. We have found that, even in most 3D formations, the component j_y may be neglected on the axis of the transmitting dipoles (at the receiver location) after the current turnoff. Then, since $\text{div}\,\mathbf{j} = 0$, we can apply Gauss's theorem $\oint \mathbf{j} \cdot ds = 0$ to the area from x to $x + \Delta x$ along the x-axis and from 0 to some Δz along z, as follows:

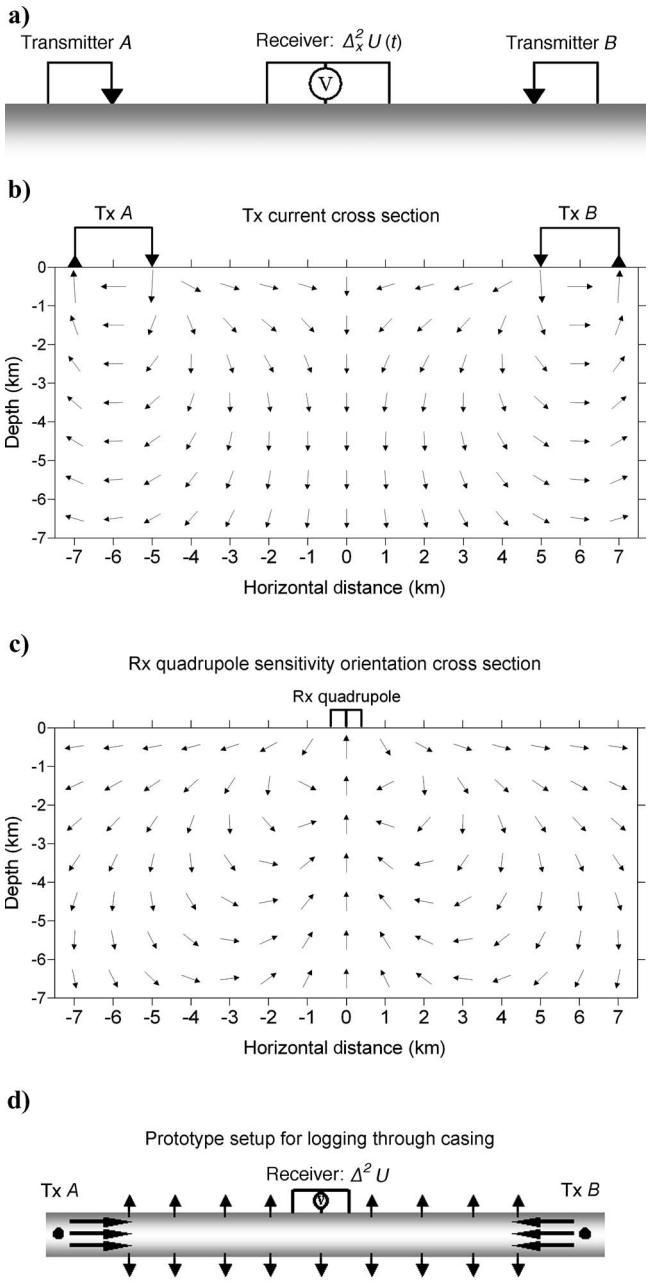

Figure 1. (a) The experimental setup with grounded electrodes (the earth is gray); (b) the dc current pattern for the transmitters and (c) the receiver; (d) the logging through casing prototype setup scheme. Arrows indicate directions of current flow. Both setups provide (a) vertical or (d) radial current focusing.

[4]Scott Urquhart furnished the current patterns for the present paper.

$$\Delta_x^2 U = \Delta_x U(x + \Delta x) - \Delta_x U(x) \sim [J_x(x + \Delta x) - J_x(x)]\Delta z = -\int_x^{x+\Delta x} J_z(x)dx, \quad (7)$$

where J_x and J_z are the linear current densities along the x- and z-directions, respectively. In other words, the quantity $\Delta_x^2 U$ is sensitive to the vertical current directed downward, from the receiver area to deep structures. In this way, the vertical current can be focused. Below, we will detail two different ways to accomplish such focusing using two transmitters. We will show that measuring $\Delta_x^2 U$ with two transmitters eliminates the effect of near-surface inhomogeneities and laterally adjacent formations, which are generally large for conventional resistivity methods.

Also note that, because of the J_z-sensitivity of $\Delta_x^2 U$, our measurements are more sensitive to vertical conductivity, rather than horizontal conductivity. This is a useful system property for vertically anisotropic rocks. Indeed, it is known that it is mainly the vertical conductivity that reflects hydrocarbon saturation (Klein et al., 1997).

The first difference $\Delta_x U$ that is commonly used to compute conventional apparent resistivity ρ_{app} (equation 6) is mainly sensitive to the current density J_x propagating along the earth in near-surface structures and hence, to the horizontal conductivity.

The $\Delta_x^2 U$ measurement with a single transmitter has an essential drawback: It is sensitive to local variations of resistivity. We show in Appendix A how we overcome this drawback.

The ideas of vertical focusing and eliminating the influence of the axial current originated in logging resistivity through steel casing (Rykhlinski, 1972). Figure 1d depicts a scheme of the setup used for logging through casing, which was a prototype for our setup. The three-electrode receiver (also measuring $\Delta^2 U$) is placed between the two transmitters. They can be either single poles or dipoles. At each logging point, the currents in the transmitters are automatically adjusted by feedback so that the axial current at the receiver location is zero. In this way, only the radial current directed into the formation is present at the receiver location. The measured signal $\Delta^2 U$ is related to this radial current (by analogy with equation 7) that is obviously proportional to the formation radial conductivity.

The method of measuring $\Delta^2 U$ for logging through casing was patented by Alpin (1939), and the use of two transmitters to eliminate the axial current at the receiver was patented by Rykhlinski (see his French patent, 1970; and its Russian counter part, 1972). However, it was difficult to utilize these ideas because they required very precise measurements, which were not available at that time. Indeed, the axial current in the steel casing can exceed by millions of times the radial current leakage into the formation. So, even though the proposed scheme suppresses the axial current, the precise cancellations required for success are not so easily accomplished. Nonetheless, recently such a tool was built successfully in Russia (Kashik et al., 2001, 2004).

Widely used in Laterolog tools, the automatic current focusing system decreases the effects of the mud column and shoulder beds (Doll, 1951; Suau et al., 1972). Kaufman (1989) also exploits similar ideas for logging through casing.

MEASURED, DIFFERENTIALLY NORMALIZED DATA

The two transmitters generate a sequence of rectangular alternating-sign low-frequency pulses with pauses between them. The durations of the pulses and the pauses should be long enough. Usually the pulses are 2, 4, or 8 s; however, they may be even longer in the marine version if the sea-water depth exceeds 100 m. Transient processes in the investigated formation should finish for these periods of time. During the off-time, at the time moments $t = t_0 + \Delta t, t_0 + 2\Delta t$, $t_0 + 4\Delta t$, etc., the following four quantities are measured at the receiver:

$$\sum_{AB} \frac{\Delta_x U(t)}{\Delta_x U(t_0)}, \quad \sum_{AB} \frac{\Delta_x^2 U(t)}{\Delta_x U(t)}, \quad \sum_{AB} \frac{\Delta_t \Delta_x^2 U(t)}{\Delta_x U(t)}, \quad \sum_{AB} \frac{\Delta_t \Delta_x^2 U(t)}{\Delta_t \Delta_x U(t)}. \quad (8)$$

By summation over A and B, we mean either the sum (first expression 8) or the difference (second–fourth expressions 8) between the two separate measurements with transmitter A or B activated (Figure 1a). We denote all expressions 8 by the sum sign. Because of the opposite signs of the transmitting currents in transmitters A and B, both terms in each expression have the same sign. So, in a 1D horizontally layered medium this is just the sum of two identical measurements. By t_0, we mean the time of the current turn-off; $\Delta_x U(t)$ and $\Delta_x^2 U(t)$ are the instantaneous values of the first and second spatial potential differences; and the following time differences are measured:

$$\Delta_t \Delta_x U(t) = \Delta_x U(t + \Delta t) - \Delta_x U(t), \quad (9)$$

$$\Delta_t \Delta_x^2 U(t) = \Delta_x^2 U(t + \Delta t) - \Delta_x^2 U(t). \quad (10)$$

When processing the data indicated by expressions 8, normalization is done by placing the potential differences in the denominator, rather than the current I, as in conventional resistivity methods (see equation 6 for the apparent resistivity). This is an important feature of our method, proposed by Rykhlinski et al. (1986a, 1986b, 1987). Dmitriev and Davydycheva (1989) and Legeido et al. (1997) show that with this method it is possible to reduce drastically the influence of both near-surface inhomogeneities and the grounded-electrodes contact impedance, and therefore obtain detailed information about deeper structures.

In our present setup, we do not use an automatic system to adjust the currents in the transmitters, as is done in logging tools (Doll, 1951; Rykhlinski, 1970, 1972; Suau et al., 1972). Because we use only the ratios in expressions 8, rather than absolute voltages, the values of the currents in the transmitters A and B are not important and do not need to be adjusted by any feedback loop. Instead, the summation of these two measurements (over A and B) eliminates the influence of local near-surface structures in the same way as the feedback loop of logging tools eliminates the influence of borehole inhomogeneities. We call this *element-by-element recording* (see Appendix A).

Let us illustrate this using a 3D modeling example (responses are computed using the finite-difference code by Druskin and Knizhnerman, 1988, 1994). Figure 2 shows the dc response of a 1 ohm-m formation including a parallelepiped block of 500-ohm-m resistivity situated at a depth of 3 km. There are also three small resistive (10 ohm-m) inclusions at a depth of 200 m, each 100 × 100 × 100 m. The formation is excited using the setup described above. The spacing (the distance between the receiver and each transmitter) is 6 km; the lengths of the transmitters are 2 km each, whereas the distances between receiving electrodes vary.

When the transmitters A and B are activated separately, it is easy to see that the quantity Δ_x^2U/Δ_xU (it does not depend on t in the dc case) measured on the surface of the formation (the upper plot) is strongly distorted by the small inclusions. However, when summing these two responses (the lower plot), the distorting influence of small inclusions is partly canceled, especially if the distance between the receiving electrodes is sufficiently large. Then the response of the deeper structure — a decreased signal above it — is clearly seen.

Figure 3 shows the same effect observed on field measurements. On the upper plot, we see two very distorted curves with the transmitters A and B activated separately, taken 0.5 s after the current turn-off. However, when summing the A and B responses, we obtain a fairly smooth curve that is suitable for interpreting, which is explained below.

All the examples below (especially the last one) illustrate the high lateral resolution of the method resulting from vertical focusing, which reduces the effect of lateral heterogeneities, though we used simple 1D modeling in complex 3D environments.

In Appendix A, we present a rigorous proof that element-by-element recording eliminates the impact of lateral variations of the conductivity in the near-surface layer, to which the second potential difference is usually very sensitive.

The subtraction of the data measured at different times, as in equations 9 and 10, contributes also to reducing the influence of near-surface inhomogeneities because the latter gets partially canceled during subtraction. Dmitriev and Davydycheva (1989, 1991) investigate a similar effect on Δ_x^2U/Δ_xU for frequency sounding of a conductive 2D formation (IP effect is absent). They show that it is possible to drastically decrease the distorting influence of near-surface 2D inhomogeneities by subtracting data taken at two different frequencies.

However, probably the most compelling feature of the quantities in expressions 8 comes from their ability to disentangle the EM and IP responses of the formation. Consider, for example, the second quantity $\Delta_x^2U(t)/\Delta_xU(t)$. While both numerator and denominator obviously decay after the current turnoff, their ratio remains fixed over a homogeneous polarizable half-space. Indeed, Kulikov and Shemyakin (1978) showed that the electric field on the surface of a homogeneous polarizable half-space is given by the following expression (the Cole-Cole model of the conductivity with $c = 0.5$ is assumed):

$$E_x(t) = \frac{P}{x^3}\left\{\left[\operatorname{erf}(u) - \frac{2u}{\sqrt{\pi}}e^{-u^2}\right] + \eta e^{n^2/u^2}\left[1 - \operatorname{erf}\left(\frac{n}{u}\right)\right] + \eta\left[\operatorname{erf}(u) - \frac{2nu}{\sqrt{\pi}}\right]e^{-u^2} + \eta e^{n^2/u^2}e^{2n}\left[1 - \operatorname{erf}\left(\frac{n}{u} + u\right)\right] \times (1 - 2n + 2n^2)\right\}, \quad (11)$$

where P is the exciting dipole moment; x is the spacing; $\operatorname{erf}(u)$ is the error function, u and n are dimensionless parameters: $u = 0.5x\sqrt{\sigma_0\mu/t}$ and $n = 0.5x\sqrt{\sigma_0\mu/\tau}$. It is not difficult to differentiate $E_x(t)$ in equation 11 with respect to x (the derivative expression for $\partial E_x(t)/\partial x$ is given by Legeido et al., 1990).

Figure 4 shows the ratio $[x\,\partial E_x(t)/\partial x]/[3E_x(t)]$, which is the continuous analog of the discrete quantity $\Delta_x^2U(t)/\Delta_xU(t)$, as a function of time t. It is easy to see that it decays soon after the current turnoff and then, after passing some minimum value, increases to some asymptotic late-time value. This happens earlier for higher values of the IP parameter η of the half-space. This asymptotic value is zero when $\eta = 0$.

The early time decaying branch of these curves reflects mainly the EM response of the half-space, which is almost independent of the IP parameters. However, the late-time increasing branch reflects the IP response of the half-space.

Figure 5 shows 1D modeling of the second quantity of expressions 8 denoted for brevity as P_x. This quantity is calculated on the surface of a five-layered medium, including a 50-m thick layer of salty water, a 950-m thick resistive layer, and a 100-m thick polarizable layer below it. The length of the transmitting dipoles is 1000 m, the length of the receiver is 250 m, and the spacing is 1500 m. The time dependence of P_x shows that the polarizable layer reveals itself starting from time $t = 1$ s. In the absence of the IP effect (red curve) P_x is practically equal to 0 for $t > 2$ s, whereas it approaches a negative late-time asymptotic value (green curve) if the IP effect is present.

Our practical measurements (see Figure 6 and Legeido et al., 1990) show that curves having nonzero late-time asymptotic are observed in several kinds of sedimentary rocks. They clearly indicate the presence of apparent polarizable structures. The depth, size, and IP parameters of the structures determine the shape of these curves, their extremum values, their late-time asymptotic values, and the time when the asymptotic is reached.

The data from expressions 8 are filtered from occasional exterior

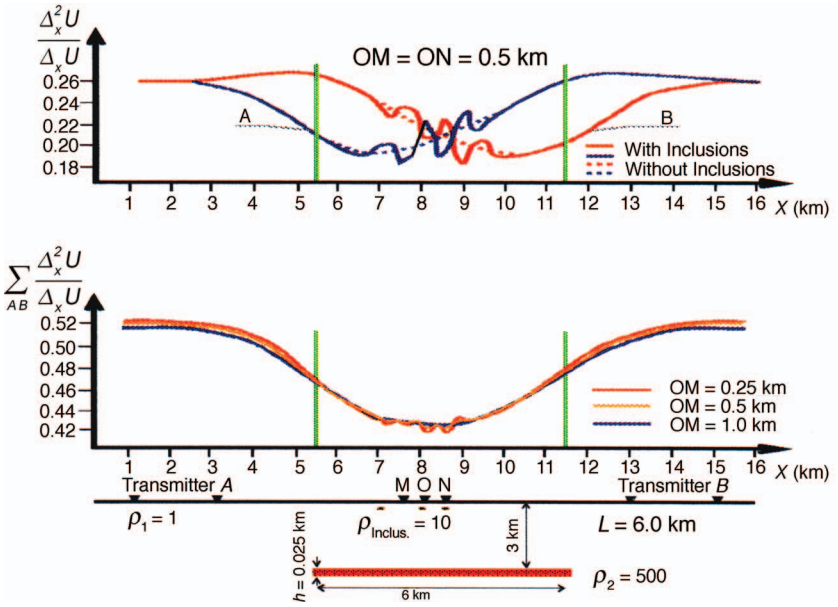

Figure 2. 3D modeling of the dc response of the formation, including one deep and three shallow resistive structures. The summation over transmitters A and B reduces the distorting influence of the shallow inclusions.

electrical noise by means of median filtering of multiple measurements from repetitions of the current pulses. Measurement accuracy must be high enough to reveal the particular features of the transient curves that are associated with the induced polarization. For this purpose, 24-bit analog-to-digital converters are used for the measurements. We use a power source of 10–20 kW in the surface version, and 500–700 kW in the marine version.

The data given by expressions 8 are measured at different moments of time t, corresponding to different penetration depths of the field.

The inverse problem of computing the IP parameters σ_0, η, τ, and c in equation 5 is solved for a 1D horizontally layered model of the medium. Such a model admits a quasi-analytical solution of problem 1. At each point of the profile along the x-axis, the inverse problem is solved independently. This is possible even in complicated 3D environments because of the vertical focusing of the current. In such a way, we get a stitched-together 2D or 3D image.

The thicknesses of the layers are computed also during the inversion. However, some a priori known parameters (for example, the thicknesses) may be specified.

The inverse algorithm minimizes the misfit functional using the ravine method (Yanovskaya and Porokhova, 1983). At the bottom of a ravine, the convergence of iterations may become slow. The ravine method allows movement along a ravine to a minimum. A description of the ravine method applied to the discussed problem can be found in Mandelbaum et al. (2002). However, other methods of the minimization of the misfit, functional for parametric inversion, also can be used: for example, the standard Gauss-Newton method using Frechet derivatives with respect to the inverted parameters.

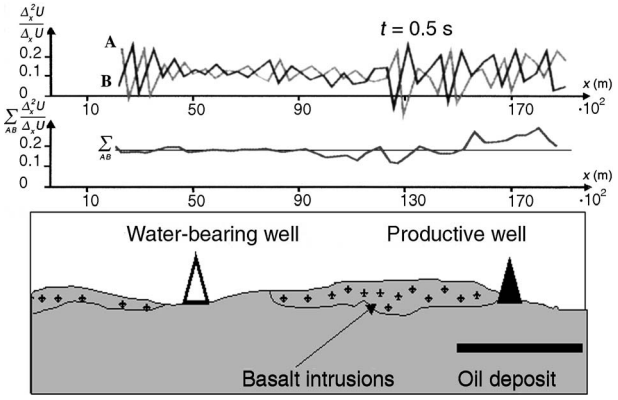

Figure 3. Field measurements taken on Verkhnechonskoe oil deposit (east Siberia). The summation over two transmitters reduces the distorting influence of the shallow inhomogeneities. Lower schematic picture shows an oil-saturated bed at $x > 15$ km at 1600 m deep.

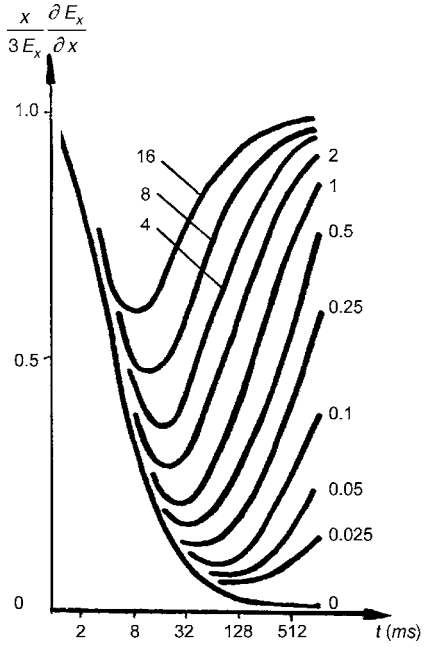

Figure 4. Time dependence of the dimensionless quantity $[x\,\partial E_x(t)/\partial x]/[3E_x(t)]$ on the surface of the homogeneous polarizable half-space after the current turn-off, for different IP coefficients η (indicated on the plot in %). The other Cole-Cole model parameters are the following: $\sigma_0 = 0.01$ S/m, $\tau = 0.1$ s, and $c = 0.5$. The spacing $x = 1.6$ km.

PRACTICAL RESULTS

The first stage of our technique development (late 1980s–early 1990s) did not involve any rigorous inversion of the Cole-Cole model parameters. We investigated mainly the quantity Δ_x^2U/Δ_xU and analyzed its behavior in both frequency and time domains. We showed that after current turn-off, Δ_x^2U/Δ_xU did not decay in all types of sedimentary rocks, but demonstrated the behavior shown in Figures 4

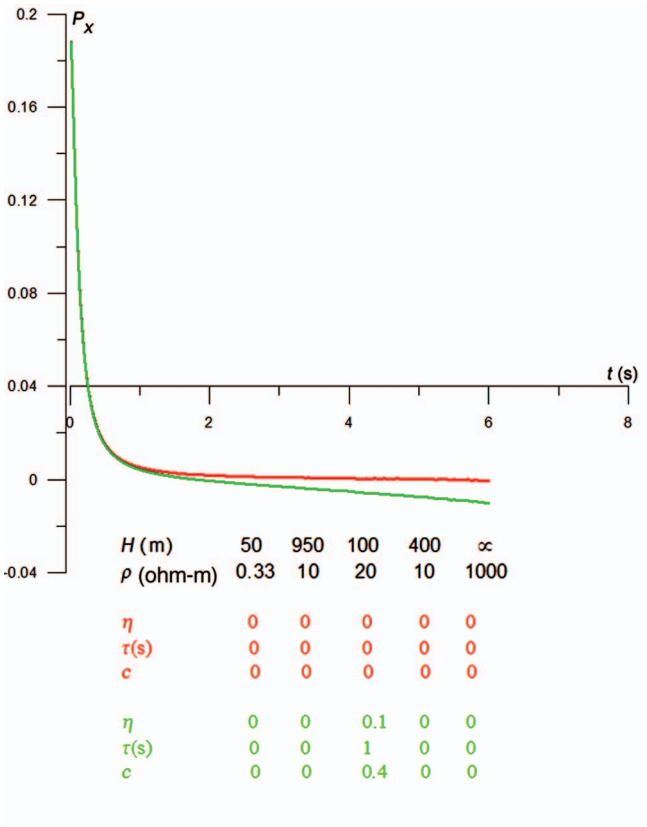

Figure 5. 1D modeling on the surface of a five-layered medium. The polarizable layer reveals itself in a few seconds after the current turn-off. In the presence of the IP effect, the dimensionsess quantity P_x approaches a negative late-time asymptotic value.

and 5. We found a correlation between hydrocarbon presence and the extremum value and the late-time asymptotic value.

We illustrate this using an example from Verkhnechonskoye oil deposit in the Irkutsk region of east Siberia. The site is located 60°20′ N and 109° E. The area of this irregularly shaped deposit is about 2000 km^2. The deposit is multistratified, gas-condensate-oil, with a structural and lithological trap, involving tectonic and lithologic sealing. Sediments consisting of carbonates and evaporites are about 2 km thick, and their total horizontal conductance, to the basalt basement, varies from 30 to 90 S. This complex structure includes multiple rock-salt layers at depths up to 1 km, and basalt intrusions, sometimes located on or close to the earth's surface. The main oil and gas pay zone is located in the basal-terrigeneous Lower-Cambrian sandstones at 1600–1700 m depth. Traditional methods, including seismic, failed to detect the deposit. Its boundary was mapped only by using the suggested method and by drilling. More than 4500 km of profiles of this area were processed using our technique, with more than 13,000 measuring stations on these profiles.

Figure 3 shows the dependence of Δ_x^2U/Δ_xU on x along a profile at time $t = 0.5$ s after current turnoff. This quantity is severely distorted (mainly by the influence of near-surface inhomogeneities, because the random oscillations have high spatial frequency). However, the second plot — the sum of those two distorted measurements — is smooth and suitable for interpretation. It shows increased values of this quantity at $x > 15$ km and suggests the presence of oil under this profile at $x > 15$ km. Indeed, the drilling data (Figure 3, bottom schematic picture) confirmed our conclusion.

Figure 6 shows an example of qualitative interpretation using the time differentiation 10. At the bottom of Figure 6, the lower part of the depicted geologic section was obtained independently from geologic, drilling, and logging data. It contains a claystone layer (argillites) and an oil-bearing sandstone under it. The upper part of the section is not shown. It contains multiple rock-salt layers and basalt intrusions.

Figure 6a shows the data $\Sigma_{AB}\Delta_x^2U/\Delta_xU$ at $t = 0.0625$ s after the current turn-off. Because the time is too short, this plot does not reflect any response from the deep oil-bearing bed. The second plot shows the same data at $t = 0.5$ s. We can see that $\Sigma_{AB}\Delta_x^2U/\Delta_xU$ increases noticeably, as compared to $t = 0.0625$ s, especially above the oil-bearing sandstone (shaded region). This occurs because of the IP time-increase effect shown Figure 4. The third plot shows the time difference, or the difference between curves a and b. It is easy to see the correlation with the presence of oil. The data were confirmed by cased well 89, drilled prior to our survey. The steel casing made reliable measurements impossible, because the measured data are very sensitive to the vertical current, according to equation 7, and therefore, to such vertical conductive structures as the casing that supports a strong vertical current. This is why we can see bad measurements and a gap in the plots about 3 km from the well. Wells 85 and 104 were drilled after our survey and confirmed our interpretation.

Figure 6d shows the time-decay curves of the measured data along the profile from 0.0625 to 0.5 s. They are the time-increase curves described in Figure 4. They show just a slight increase of time in the area of the dry well and a strong increase above the oil reservoir.

The prediction using our method on the Verkhnechonskoye oil deposit was confirmed by the results of 64 drilled boreholes. Only two of them, placed too close to the deposit boundary, did not confirm the predicted result. Maps and more detail of this deposit can be found in Legeido et al. (1990 and 1997).

Presently, we are conducting rigorous 1D inversion to image the IP parameters using the four DNM data in expressions 8. Figure 7 shows an example of IP imaging along a profile in another site on the Ob Estuary (west Siberia), crossing it perpendicularly at the midpoint. Images of the resistivity $1/\sigma_0$, the IP parameter η, and the time-decay constant τ are shown. The horizontal axis indicates the x-coordinate of the profile, whereas the vertical axis is depth z. The two ellipses indicate two zones of higher η and τ, which correlate with the hydrocarbon presence. A borehole was drilled at $x = 25$ km, and an upper commercial gas reservoir and a lower noncommercial oil reservoir were revealed at depths 1150 m and 1900 m, respectively. The thickness of the gas-bearing sandstone is about 40 m, whereas the thickness of the lower oil-bearing bed does not exceed 20 m, according to logging data. Both reservoirs were detected using only the suggested method.

The resistivity image in Figure 7 does not have such a clear anomaly in the area of the oil deposits, as η and τ. However, the resistivity image still demonstrates high spatial resolution. The green color corresponds to the resistive, very fresh water of the Ob River and underlying rocks. The two red areas of higher resistivity, up to 900 ohm-m, are located from 2 to 6.5 km and from 26.5 to 33 km along x, at depths from 0 to 0.4 km. They correspond to the two coastal permafrost zones of the Ob Estuary.

It is possible to see an area of low resistivity at a depth of about 2 km (dark blue color). This corresponds to the location of the oil and mineralized water trap. As logging data showed, the oil saturation in the lower deposit is not of commercial value. This agrees with our imaging results. In the area of the second ellipse at deeper depth, we see even slightly decreased resistivity, probably resulting from salty water, though the other IP parameters are increased.

The parameter c (relaxation constant in equation 5) for this example was inverted also. However, it is not shown because it did not re-

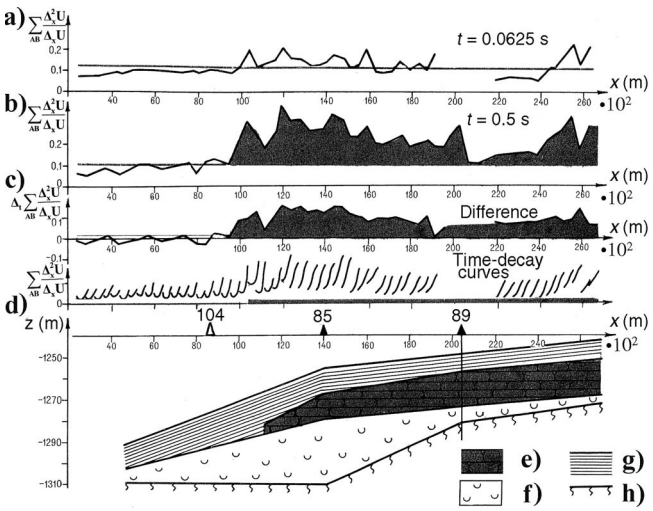

Figure 6. Qualitative interpretation of geologic data from the Verkhnechonskoe oil deposit: (a) The measurements taken at 0.0625 s after the current turnoff; (b) the same, at 0.5 s; (c) the difference of those two measurements; (d) the time-decay curves on the interval from 0.0625 to 0.5 s. (e) Oil-bearing sandstone (shaded); (f) erosion zone of the basalt basement; (g) argillites; (h) basalt basement. The productive cased well is 89, the productive uncased well is 85, and 104 indicates the water-bearing well. Shading indicates the oil. Depths are given from sea level; earth's surface is at 400 m above it. Spacings: 800 m.

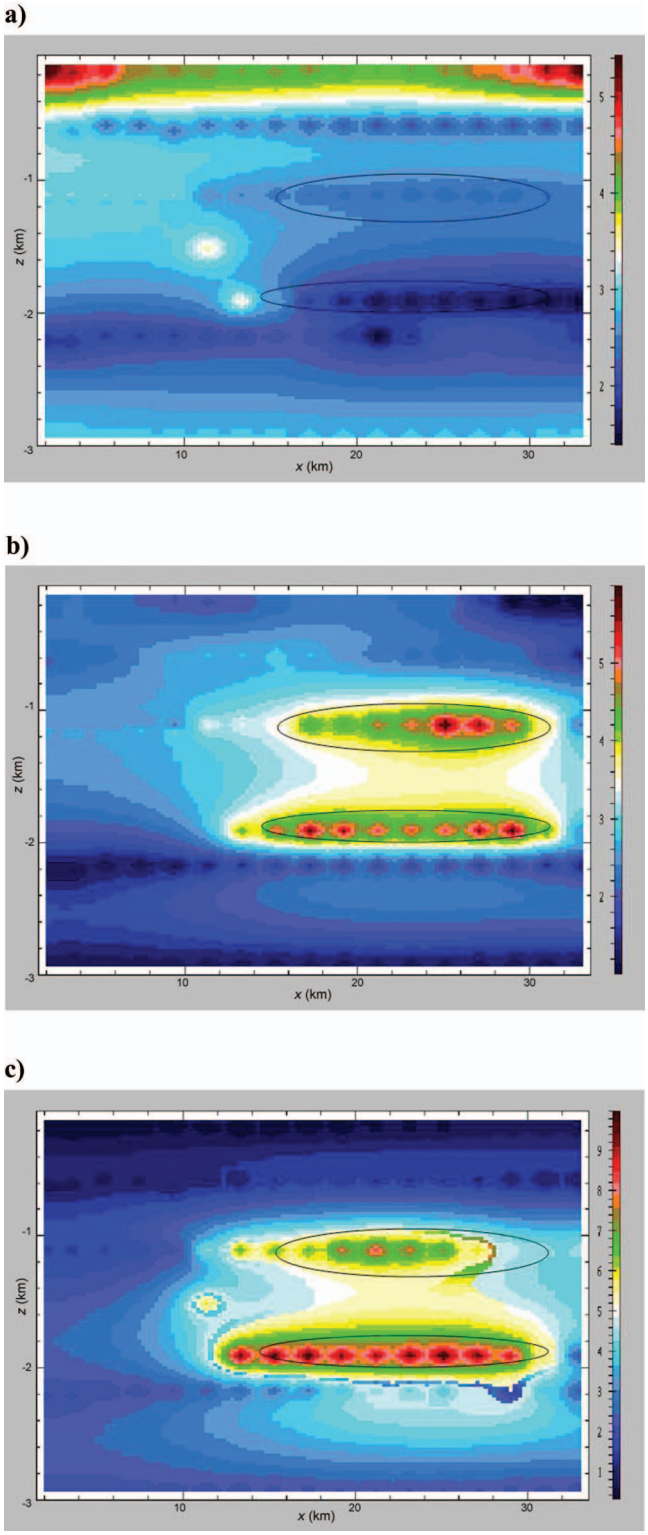

Figure 7. The images of (a) the resistivity $1/\sigma_0$ in logarithmic scale, in ohm-m, (b) the IP parameter η, in %, and (c) the time-decay constant τ in tenths of a second. The color in (a) shows $\ln(1/\sigma_0)$. The brown-red color (up to 300 ohm-m in the picture) corresponds to the permafrost zones under the coasts of the Ob estuary. The dark blue color (a few ohm-m) corresponds to the oil-water trap. Spacings: 2 km.

veal, in this case, any clear correlation with the real geologic structures. According to our investigations, it usually varies in the range of 0.1 to 0.9 and hardly reflects hydrocarbon saturation.

The last example shown in Figures 8 and 9 also demonstrates high lateral and vertical resolution of the suggested method. Figure 8 shows a map of the Bratsk gas-condensate deposit, Irkutsk Region,

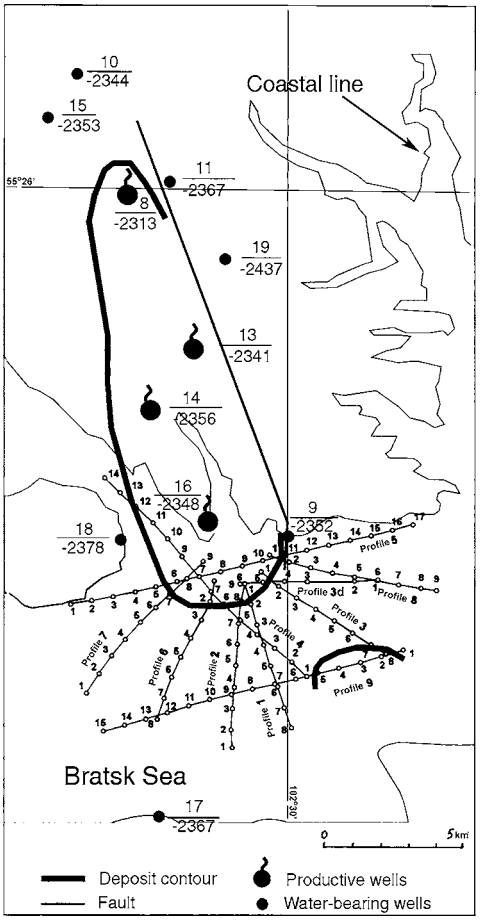

Figure 8. Map of Bratsk gas-condensate deposit with DNM profiles on the Bratsk Sea water surface.

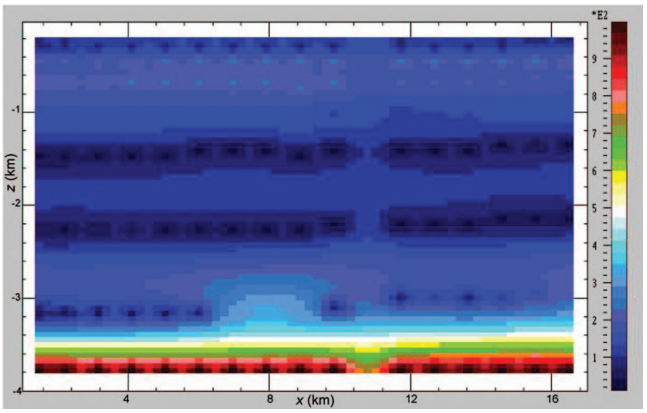

Figure 9. Image of the resistivity $1/\sigma_0$ in linear scale, in ohm-m, along profile 5. A basalt basement, a gas reservoir, three resistive rock-salt layers, and a vertical fault can be distinguished in the image. Spacings: 800 m.

east Siberia (55° N and 102.5° E). The deposit is embedded within the basal Lower Cambrian horizon of terrigeneous sediments. At a depth of 3400 m, the horizon contains a sandstone layer, about 15 m thick. The layer has a low resistivity (a few ohm-m) in its water-bearing part and is more resistive (tens of ohm-m) in its productive part. Below it, starting from a depth 3400 m, is a highly resistive basalt basement. This description is based on drilling and logging of four gas-bearing wells (8, 13, 14, and 16 on the map) and seven water-bearing wells (9, 10, 11, 15, 17, 18, and 19). The thick line shows the contour of the deposit. The thin straight line shows a geologic fault, which was revealed by logging data of wells 9 and 11. Multiple nearly straight lines with circles, on the Bratsk Sea water surface, signify profiles of the survey with measuring stations.

Figure 9 shows the image of the resistivity $1/\sigma_0$ under profile 5. It agrees with the drilling and logging data partly presented on the map. It is easy to distinguish the high-resistive basalt foundation (red) and the gas reservoir (light blue color from $x = 6.4$ km to $x = 10$ km, compared to the darker blue region indicating the absence of gas). The reservoir is located in the basal sandstone at a depth of 3400 m below sea level, or 3800 m from the earth's surface. This is confirmed by drilling and logging data of wells 18 (at $x = 5$ km, water-bearing), 16 (at $x = 8$ km, gas-bearing), and 9 (at $x = 11$ km, water-bearing). Unfortunately, the survey was performed only from the water surface because of very thick forest on the remaining surface area above the reservoir.

Dark- and lighter-blue horizontal stripes can also be seen in Figure 9. They correspond to water-saturated sandstone embedded with multiple rock-salt layers mixed with dolomites, revealed by drilling at depths from 900 to 1100 m, from 1700 to 2000 m, and from 2400 to 2600 m. Moreover, the vertical fault at $x = 11$ km also can be seen from a depth of 1400 to 3800 m. Such a high lateral resolution is achieved by vertical focusing of the electric current and the elimination of the effect of laterally adjacent formations (known in the logging community as the shoulder effect).

Other IP parameters for this example were inverted, too. However, in this case, they did not contrast in the gas reservoir area, unlike resistivity. A possible explanation could be related to the dependence of the IP parameters of the type and saturation of hydrocarbons. We suggest that oil saturated rocks may have larger IP parameters η and τ, compared to gas-saturated rocks.

Although the last example supports the IP method because of the low contrast of the IP parameters, we would not be able to provide the resistivity image without taking all of them into account. In this case, we also observed the V-type curves of the measured data whose nature is related to the IP effect.

DISCUSSION

As noted in the introduction, organic electrochemistry is not well studied, compared to other types of reactions that cause the IP effect. Olhoeft (1985) suggests that it is unlikely that the full nature of such reactions will ever be known. Still, there is insufficient study of how the IP parameters correlate with hydrocarbon saturation.

Vinegar and Waxman (1984) claim that the complex conductivity (both real and imaginary) of oil-bearing rocks is less than the conductivity of water-bearing rocks. This is quite obvious for the real part of conductivity. However, the behavior of its imaginary part, which indicates the IP effect, may be more complicated. Olhoeft (1985) states that organic contamination of rocks shifts the low-frequency phase response to a lower frequency. This statement agrees with our observations: We revealed that hydrocarbon-saturated rocks have a greater time-decay constant τ (see Figure 7) that corresponds to the lower frequencies of the conductivity spectrum.

Kemna et al. (2004) also report progress in using the IP effect for hydrocarbon-contaminant mapping and imaging. They detected an increased imaginary conductivity and especially an increased phase shift of the complex conductivity in the area of the former jet-fuel depot near the Strasbourg-Entzheim Airport in France, where the soil is contaminated with kerosene.

Dias (2000) analyzes several models of conductivity expressed as a function of frequency. He compares the behavior of the amplitude and phase shift of the IP potential as a function of frequency using experimental laboratory measurements on synthetic samples of sedimentary rock. He reports that only two models — the Dias model (a function of frequency and seven independent parameters) and the multi-Cole-Cole model (five independent parameters) — can fit the experimental data. He claims that all other models, including Cole-Cole (four independent parameters), fail to describe the phase-shift data.

However, increasing the number of the independent parameters really complicates the inversion of the rock electrical properties. Some additional measured data are needed to invert more than four parameters. Thus, a reasonable compromise should be found between model complexity and data density.

We believe that the Cole-Cole model provides such a compromise. Unfortunately, as far as we know, there is a lack of published data showing how the parameters of the Cole-Cole model (or other quantitative models) reflect the presence of hydrocarbons. But the field tests presented here reveal correlation between IP parameters and the presence of hydrocarbons.

There remain many unsolved problems related to the IP effect that require more research. Special electrochemical investigations are needed to explain the complex nature of the IP. Rigorous 3D inversion of the IP parameters of geologic formations should be done.

However, the IP-prospecting technology proposed in this paper is inexpensive. The method can provide interesting data about the formation and does not require expensive well drilling. We believe that it will enable us to complete the challenging and complicated task, suggested by J. R. Wait, of exploiting the IP effect as a rich source of data about formations.

CONCLUSION

Based on the suggested method, the investigation of a large number of hydrocarbon deposits has established that when hydrocarbon-bearing rocks are present, the IP parameters image the formation. They reflect anomalies at the correct depth, regardless of the trap type and its geometry. Different IP parameters show different sensitivities to inferred hydrocarbon type and saturation.

Thus, we report significant progress in geophysical prospecting of oil and gas deposits. In all regions investigated, our method demonstrates high resolution and allows detecting boundaries of hydrocarbon-bearing beds in both lateral and vertical directions. We revealed that neither high-resistive permafrost zones, low-resistive salty water, nor multiple rock-salt beds are obstacles for the wave-propagation processes excited in the presence of the IP effect. This occurs because of the huge, effective dielectric constant of oil-saturated rocks and the consequent generation of displacement currents.

ACKNOWLEDGMENTS

The authors are indebted to Vladimir Druskin (now at Schlumberger) for help in solving the forward problem, to Tom Barber, Christian Besson, Robert Freedman, Richard Rosthal, Jan Smits, Andrea Zerilli (Schlumberger), J.-B. Clavaud, Vladimir Dmitriev, Alexander Kaufman, and Frank Morrison for useful discussions. Extensive editing by Mark Everett, Scott Urquhart, and four anonymous referees significantly improved the quality of the manuscript.

APPENDIX A

ELEMENT-BY-ELEMENT RECORDING IN 3D MEDIA

Let us consider the behavior of the differential analog of the quantity $\Sigma_{AB} \frac{\Delta_x^2 U}{\Delta_x U}$ on the earth's surface. We assume fully 3D resistivity $\rho(x,y,z)$ at $z > 0$. We excited the medium by the left dipole A (see Figure 1a) and apply Ohm's law to the volume element $\Delta x \times \Delta y \times \Delta z$ adjacent to the earth's surface. Then we get

$$\Delta_x U(A) = I_x(A)\rho(x,y,z)\Delta x/(\Delta z \Delta y), \tag{A-1}$$

where $I_x(A)$ is the x-directed current from the transmitter A. Then, assuming Δx is small enough, we get the following:

$$\frac{dU(A)}{dx} = I_x(A)\frac{\rho(x,y,z)}{\Delta z \Delta y}. \tag{A-2}$$

Differentiating equation A-2 with respect to x, we arrive at the expression

$$\frac{d^2U(A)}{dx^2} = j_z(A)\frac{\rho(x,y,z)}{\Delta z} + \frac{\partial\, \rho(x,y,z)}{\partial\, x}\frac{I_x(A)}{\Delta z \Delta y}, \tag{A-3}$$

because, according to Gauss's theorem,

$$\Delta_x I_x(A) = j_z(A)\Delta x \Delta y \Rightarrow dI_x(A)/dx = j_z(A)\Delta y. \tag{A-4}$$

Here we have neglected the y-directed current on the earth's surface during the off-time (Zhdanov and Keller, 1994, p. 369).

It is easy to see from equation A-3 that the second derivative of the electric potential may be very sensitive to lateral variations of the resistivity.

Dividing equation A-3 by equation A-2 we arrive at the following equation:

$$\frac{d^2U(A)/dx^2}{dU(A)/dx} = \frac{j_z(A)}{dU(A)/dx}\frac{\rho(x,y,z)}{\Delta z} + \frac{1}{\rho(x,y,z)}\frac{\partial\, \rho(x,y,z)}{\partial\, x}. \tag{A-5}$$

Now, excite the medium by the dipole B. By analogy with equation A-5, we obtain:

$$\frac{d^2U(B)/dx^2}{dU(B)/dx} = \frac{j_z(B)}{dU(B)/dx}\frac{\rho(x,y,z)}{\Delta z} + \frac{1}{\rho(x,y,z)}\frac{\partial\, \rho(x,y,z)}{\partial\, x}. \tag{A-6}$$

Taking a difference of expressions A-5 and A-6, we arrive at the following:

$$\sum_{AB} \frac{d^2U/dx^2}{dU/dx} = \left(\frac{j_z(A)}{dU(A)/dx} - \frac{j_z(B)}{dU(B)/dx}\right)\frac{\rho(x,y,z)}{\Delta z}. \tag{A-7}$$

As mentioned, we call it a *sum*, because both terms have the same sign as a result of the opposite directions of the currents from the dipoles A and B.

It is easy to see that expression A-7 does not contain the derivative $\partial\rho(x,y,z)/\partial x$, as do expressions A-5 and A-6. Thus, the effect of the horizontal current is completely canceled, and the effect of the vertical current is duplicated (because the voltages $dU(A)/dx$ and $dU(B)/dx$ have opposite signs between the transmitters). With this method, we manage to get rid of the sensitivity to the lateral variations of the resistivity in the near-surface layer and to image clearly the deeper structures. This allows us to simple 1D modeling, even in complicated 3D environments. Figures 2 and 3 illustrate this principle.

REFERENCES

Allaud, L. A., and M. H. Martin, 1977, Schlumberger: The history of a technique: John Wiley and Sons.

Alpin, L. M., 1939, The method of the electric logging in the borehole with casing: USSR Patent 56 026.

Cole, K. S., and R. H. Cole, 1941, Dispersion and absorption in dielectrics: Journal of Chemical Physics, **6**, 42–52.

Dey, A., and F. Morrison, 1973, Electromagnetic coupling in frequency and time-domain induced-polarization surveys over a multilayered earth, Geophysics, **38**, 380–405.

Dias, C. A., 2000, Development in a model to describe low-frequency electrical polarization of rocks: Geophysics, **65**, 437–451.

Dmitriev, V. I., and S. N. Davydycheva, 1989, Mathematical modeling of differential methods of frequency electric prospecting: Soviet Geology and Geophysics (Translated from Russian), **30**, 101–107.

———, 1991, Integral equation method for calculating H-polarized anomalous field: Computational Mathematics and Modeling, **2**, 288–297.

Doll, H. G., 1951, The Laterolog: A new resistivity logging method with electrodes using an automatic focusing system: Petroleum Transactions: AIME, **192**, 305–316.

Druskin, V., and L. Knizhnerman, 1988, A spectral semi-discrete method for the numerical solution of 3D non-stationary problems in electrical prospecting (in Russian): Izvestiya Academii Nauk USSR Fizika Zemli, **24**, 63–74.

———, 1994, Spectral approach to solving three-dimensional Maxwell's diffusion equations in the time and frequency domains: Radio Science, **29**, 937–953.

Freedman, R., and J. P. Vogiatzis, 1986, Theory of induced-polarization logging in a borehole: Geophysics, **51**, 1830–1849.

Fuller, B. D., and S. H. Ward, 1970, Linear system description of the electrical parameters of rocks: IEEE Transactions on Geoscience Electronics, GE-8, **1**, 7–18.

Kashik, A. S., N. I. Rykhlinski, G. N. Gogonenkov, R. I. Krivonosov, and V. Z. Garipov, 2001, A method of electrical logging of cased wells (in Russian): Russian Patent 2 176 802, Bulletin of Inventions, 34.

Kashik, A. S., N. I. Rykhlinski, L. A. Knizhnerman, R. I. Krivonosov, and A. S. Stepanov, 2004, On a problem of the wireline electric logging of wells with steel casing: Karotazhnik, **3–4**, 116–117; EAGE Press (in Russian), 8–23.

Kaufman, A. A., 1989, Conductivity determination in formation having a cased well: U. S. Patent 4 796 186.

Kemna, A., A. Binley, and L. D. Slater, 2004, Crosshole IP imaging for engineering and environmental applications: Geophysics, **69**, 97–107.

Klein, J. D., P. R. Martin, and D. F. Allen, 1997, The petrophysics of electrically anisotropic reservoirs: The Log Analyst, **39**, 25–36.

Klein, J. D., and W. R. Sill, 1982, Electrical properties of artificial clay-bearing sandstone: Geophysics, **47**, 1593–1605.

Komarov, V. A., 1980, Electric survey by the induced polarization method (in Russian): Nedra.

Kormil'tsev, V. V., and A. N. Mezentsev, 1989, Electric prospecting in polarizable media (in Russian): Ural Branch of Academy of Sciences USSR.

Kulikov, A. V., and E. A. Shemyakin, 1978, Electrical survey by phase method of induced polarization (in Russian): Nauka.

Legeido, P. Y., M. M. Mandelbaum, and N. I. Rykhlinski, 1990, Application

of differentially adjusted electric exploration of the Nepa Dome: Soviet Geology and Geophysics (translated from Russian), **31**.
———, 1997, Results of differential-normalized electrical prospecting in the Central part of the Nepa arch on the Siberian platform: Russian Geology and Geophysics (translated from Russian), **38**.
Mandelbaum, M. M., E. B. Ageenkov, P. Y. Legeido, P. Y. Pesterev, and N. I. Rykhlinski, 2002, Normalized-differential electrical measurements in hydrocarbon exploration: The state of the art and prospects for future: Russian Geology and Geophysics (translated from Russian), **43**, 1085–1143.
Marshall, D. I., and T. R. Madden, 1959, Induced polarization, a study of its causes: Geophysics, **24**, 790–816.
Mikhailov, G. N., I. P. Yurgens, and B. V. Yagovkin, 1973, Manual on induced polarization method (in Russian): Nedra.
Olhoeft, G. R., 1985, Low-frequency electrical properties: Geophysics, **50**, 2492–2503.
Pelton, W. H., S. H. Ward, P. C. Hallof, W. R. Sill, and P. H. Nelson, 1978, Mineral discrimination and removal of inductive coupling with multifrequency IP: Geophysics, **43**, 588–603.
Pirson, S. J., 1982, Progress in magnetoelectric exploration: Oil and Gas Journal, **80**.
Rykhlinski, N. I., 1970, Dispositif pour le carottage divergent de trous de forage. Republic of France Patent (Brevet d'Invention: French Patent 122 123 and 1 592 075, Bulletin official de la Propriete industrielle, 25.
———, 1972, A method of divergence logging in the borehole (in Russian): USSR Patent 333 514, Bulletin of Inventions, **11**.
Rykhlinski, N. I., S. N. Davydycheva, A. S. Kashik, V. L. Druskin, P. Y. Legeido, and V. I. Dmitriev, 1986a, A method of surface electromagnetic sounding to investigate 3D formation (in Russian): USSR Patent 1 454 101.
Rykhlinski, N. I., S. N. Davydycheva, P. Y. Legeido, M. M. Mandelbaum, and A. S. Lisin, 2004a, A method of marine geoelectrical survey (in Russian): Russian Patent 2 236 028, Bulletin of Inventions, 25.
Rykhlinski, N. I., S. N. Davydycheva, P. Y. Legeido, M. M. Mandelbaum, and E. N. Rykhlinskaya, 2003, A method of geoelectrical survey (in Russian): Russian Patent 2 219 568, Bulletin of Inventions, 35.
———, 2004b, A method of geoelectrical survey (versions) (in Russian): Russian Patent 2 231 089, Bulletin of Inventions, 17.
———, 2004c, A method of geoelectrical survey (versions) (in Russian): Russian Patent 2 235 347, Bulletin of Inventions, 24.
Rykhlinski, N. I., A. S. Kashik, V. L. Druskin, and V. P. Bubnov, 1986b, A method of surface electrical axial sounding (in Russian): USSR Patent 1 223 180, Bulletin of Inventions, 13.
Rykhlinski, N. I., A. S. Kashik, and M. M. Mandelbaum, 1987, A method of geoelectrical survey (in Russian): USSR Patent 1 436 675.
Schlumberger, C., 1920, Etude sur la prospection electrique du sous-sol: Gauthier-Villars et Cie.
Seigel, H. O., 1959, Mathematical formulation and type curves for induced polarization: Geophysics, **24**, 547–565.
———, 1974, The magnetic induced polarization (MIP) method: Geophysics, **39**, 321–339.
Slater, L. D., and D. R. Glaser, 2003, Controls on induced polarization in sandy unconsolidated sediments and application to aquifier characterization: Geophysics, **68**, 1547–1558.
Suau, J., P. Grimaldi, A. Poupon, and P. Souhaite, 1972, The dual laterologrxo tool: Annual Technical Conference of the Society of Petroleum Engineers of AIME, SPE, SPE 4018.
Ulrich, C., and D. Slater, 2004, Induced polarization measurements on unsaturated, unconsolidated sands: Geophysics, **69**, 762–771.
Vanyan, L. L., 1965, Principles of the electromagnetic soundings (in Russian): Moscow, Nedra.
Vinegar, H., J., and M. H. Waxman, 1984, Induced polarization of shaly sands: Geophysics, **49**, 1267–1287.
Wait, J. R., 1982, Geo-electromagnetism: Academic Press Inc.
Yanovskaya, T. B., and L. N. Porokhova, 1983, Inverse problems of geophysics: Leningrad University Press.
Zhdanov, M. S., and G. V. Keller, 1994, The geoelectrical methods in geophysical exploration: Methods in Geochemistry and Geophysics, **31**, Elsevier Science Publ. Co., Inc.